Cell Insight 3 (2024) 100182

Contents lists available at ScienceDirect

Cell Insight

journal homepage: www.journals.elsevier.com/cell-insight

Research Article

The cell fates of intermediate cell population in prostate development

Xiaoyu Zhang [a,b,1], Jian Wang [a,b,1], Wangxin Guo [a,c,**], Hongjiong Zhang [a,b], Bin Zhou [a,d,e], Chen Yu [c], Dong Gao [a,c,*]

[a] Key Laboratory of Multi-Cell Systems, Shanghai Key Laboratory of Molecular Andrology, Shanghai Institute of Biochemistry and Cell Biology, Center for Excellence in Molecular Cell Science, Chinese Academy of Sciences, Shanghai, 200031, China
[b] University of Chinese Academy of Sciences, Beijing, 100049, China
[c] Institute of Cancer Research, Shenzhen Bay Laboratory, Shenzhen, 518132, China
[d] School of Life Science and Technology, ShanghaiTech University, Shanghai, 201210, China
[e] Key Laboratory of Systems Health Science of Zhejiang Province, School of Life Science, Hangzhou Institute for Advanced Study, University of Chinese Academy of Sciences, Hangzhou, 310024, China

HIGHLIGHTS

- Generation of advanced, comprehensive lineage tracing strategies to investigate cell fate in prostate development.
- Demonstration that intermediate cells function as multipotent prostate stem cells in the prostate during development.
- Identification the transition of prostate intermediate cell to neuroendocrine cell during postnatal prostate development.

GRAPHICAL ABSTRACT

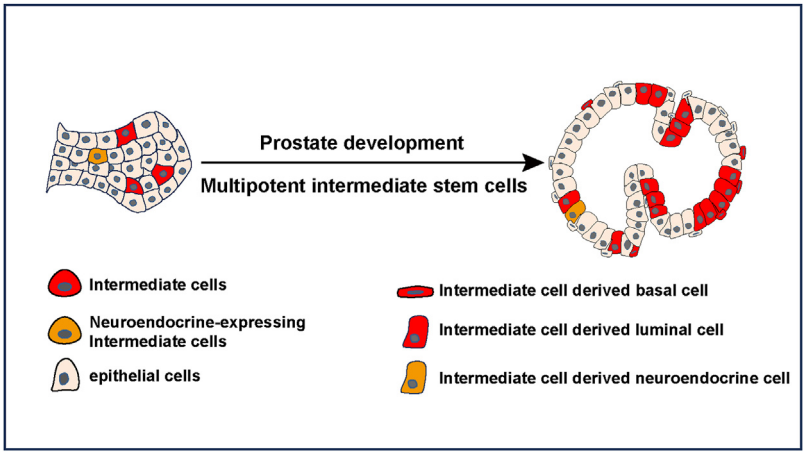

ARTICLE INFO

Keywords:
Intermediate cells
Prostate development
Stem cell
Lineage tracing

ABSTRACT

Organ development, regeneration and cancer initiation are typically influenced by the proliferation and lineage plasticity of tissue-specific stem cells. Prostate intermediate cells, which exhibit characteristics of both basal and luminal cells, are prevalent in pathological states and during organ development. However, the identity, fate and function of these intermediate cells in prostate development are not well understood. Through single-cell RNA-seq analysis on neonatal urogenital sinus tissue, we identified intermediate cells exhibiting stem cell potential. A notable decline in the population of intermediate cells was observed during prostate development. Prostate intermediate cells were specifically labeled in early and late postnatal development by the enhanced dual-

* Corresponding author. Key Laboratory of Multi-Cell Systems, Shanghai Key Laboratory of Molecular Andrology, Shanghai Institute of Biochemistry and Cell Biology, Center for Excellence in Molecular Cell Science, Chinese Academy of Sciences, Shanghai, 200031, China.
** Corresponding author. Institute of Cancer Research, Shenzhen Bay Laboratory, Shenzhen, 518132, China.
E-mail addresses: guowangxin6@sibcb.ac.cn (W. Guo), dong.gao@sibcb.ac.cn (D. Gao).
[1] These authors contributed equally to this work.

https://doi.org/10.1016/j.cellin.2024.100182
Received 23 May 2024; Received in revised form 27 June 2024; Accepted 28 June 2024

recombinase-mediated genetic tracing systems. Our findings revealed that these cells possess significant stem cell capabilities as demonstrated in organoid formation and cell fate mapping assays. These intermediate cells also exhibited intrinsic bipotential properties, enabling them to differentiate into both basal and luminal cells. Additionally, we discovered a novel transition from intermediate cell expressing neuroendocrine markers to neuroendocrine cell during prostate development. This study highlights intermediate cells as a crucial stem cell population and enhances our understanding of their role in prostate development and the plasticity of prostate cancer lineage.

1. Introduction

Prostate disease progression, including prostate cancer, potentially reawaken some developmental patterns similar to prostate development (Pletcher & Shibata, 2022; Vickman et al., 2020). The typical normal adult prostate primarily consists of basal, luminal, and rare neuroendocrine cells (Li & Shen, 2019; Shen & Abate-Shen, 2010). In addition to these primary cell types, there is a notable presence of intermediate cells, which express markers of both basal and luminal cells and are commonly observed during prostate development and in various disease conditions (Liu et al., 2016; Ousset et al., 2012; Sfanos et al., 2018; Shibata et al., 2020; van Leenders et al., 2000, 2003). Recently, several studies have pinpointed the intermediate cells as potential prostate stem cells involved in prostate regeneration, inflammation, and tumor initiation and progression (Feng et al., 2023; Guo et al., 2023; Kwon et al., 2014). Additionally, intermediate cells have been recognized as a distinct subpopulation within the human prostate that accelerates the progression of prostate cancer (Chan et al., 2022; Chen et al., 2021; Deng et al., 2022; Germanos et al., 2022; Labrecque et al., 2019; Song et al., 2022). However, the exploration of prostate intermediate cells during development has been limited to a few cell markers and transient detection in lineage tracing systems, leaving their properties and roles in organogenesis largely undefined due to technical constraints.

It is widely acknowledged that the maintenance of prostate homeostasis and androgen-mediated regeneration primarily depend on unipotent basal and luminal stem cells (Centonze et al., 2020; Choi et al., 2012; Guo et al., 2020; Wang et al., 2013), though the extent of lineage plasticity in postnatal prostate development remains debated (Pletcher & Shibata, 2022; Toivanen & Shen, 2017). Previous lineage tracing studies have shown the presence of multipotent basal stem cells during postnatal prostate development, while predominantly unipotent luminal progenitor cells have been observed (Ousset et al., 2012; Tika et al., 2019; Wuidart et al., 2016). A recent study also revealed that $Ck8^+$ luminal cells can differentiate into both basal and luminal cells, suggesting the persistence of bipotent luminal stem cells in early postnatal development (Shibata et al., 2020). Notably, single recombinase-based lineage tracing assays face technical challenges in distinguishing between separate populations of basal, luminal, and intermediate cells, leaving the cell identity and lineage plasticity of intermediate cells unclear. Moreover, the cellular characteristics and behaviors of neuroendocrine cells in prostate development are largely unknown. Neuroendocrine cells were thought to potentially originate from basal stem cells (Ousset et al., 2012; Pignon et al., 2013; Wang et al., 2020). In the context of advanced prostate cancer, luminal cells have been shown to reprogram into neuroendocrine prostate cancer (NEPC) cells through lineage plasticity (Davies et al., 2018; Han et al., 2022; Mu et al., 2017; Zou et al., 2017), indicating that luminal cells might transform into neuroendocrine cells. Thus, further research is needed to explore the lineage plasticity of prostate epithelial stem cells and to better understand the cell identity and lineage transitions of neuroendocrine cells.

In this study, we characterize the neonatal prostate epithelial population using single-cell RNA-seq (scRNA-seq) and identified potential intermediate stem cells. By applying enhanced lineage tracing strategies that utilize dual recombinases (Cre and Dre) in organoid formation and cell fate tracing assays during neonatal, early postnatal and late postnatal development, we demonstrated that intermediate cells are bipotent progenitor cells during prostate development. More notably, we discovered a neuroendocrine transition of basal, luminal, and neuroendocrine triple-positive cells to neuroendocrine cells from the neonatal stage to adulthood.

2. Results

2.1. Characterization of intermediate cell population during prostate development

To investigate the identity of epithelial stem cell in the development prostate, we conducted scRNA-seq on 6868 cells collected from urogenital sinus of 9 wild-type (WT) neonatal mice at postnatal day 0 (P0). Utilizing *t*-distributed stochastic neighbor embedding (*t*-SNE) cluster analysis, we identified 12 distinct cell clusters, including epithelial, stromal, and other cell populations (Fig. 1A and Fig. S1). Further analysis was specifically targeted at the epithelial populations to better understand their role in postnatal prostate development. By extracting and re-analyzing these epithelial cells, we annotated three distinct epithelial subsets based on marker gene expression, including an intermediate cell subset, a urethra cell subset, and a seminal vesicle cell subset (Fig. 1B). The seminal vesicle cell subset was characterized by high expression of *Pax2* and *Pax8* (Fig. 1C and Fig. S2C), while the urethra epithelial cell subpopulation prominently expressed *Tacstd2* and *Krt4* (Fig. 1C and Fig. S2B). Crucially, the intermediate cell cluster, expressing *Nkx3.1* was identified as a prostate buds-enriched epithelial population in neonatal mice (Bhatia-Gaur et al., 1999; Kruithof-de Julio et al., 2013) (Fig. 1C and Fig. S2A). These intermediate cells also exhibited expression of classical basal cell genes such as *Trp63*, *Ck5*, and luminal cell genes *Ck8* and *Ck18*, indicating their basal-luminal intermediate properties (Fig. 1D). Functionally, the intermediate cell cluster was enriched in processes such as cell proliferation, tissue development, and branching morphogenesis, suggesting that these cells possess epithelial stem cell characteristics (Fig. 1F). Furthermore, these cells displayed highly proliferative profiles with enhanced S and G2/M phase signatures, reinforcing the notion that they may function as stem cells (Fig. 1E). Additionally, using co-immunofluorescence staining for the luminal cell markers (Ck8 and Ck18) and basal cell markers (Trp63, Ck5 and Ck14), we discovered that the epithelial cells in prostate buds are intermediate cells that are co-express basal and luminal cell markers (Fig. 1G).

To explore the dynamics of these intermediate cells during prostate development, we traced the changes in epithelial cell lineage from the early postnatal stages (P0 and P7) through to late postnatal stage (P14) and into adulthood. Initially, $Ck5^+/Ck8^+$ intermediate cells constituted a significant proportion of the neonatal prostate epithelial cells (Fig. S3A, C). However, there was a rapid decrease in these $Ck5^+/Ck8^+$ intermediate cells during the early postnatal stage (from 99.0% ± 0.16% to 14.8% ± 3.30%), with a further reduction observed in late postnatal development (7.9% ± 2.60%) (Fig. S3A, C). A similar trend of rapid reduction of $Trp63^+/Ck8^+$ intermediate cells was observed across these stages of prostate development (Fig. S3B, D). As the prostate matured, specialized basal and luminal cell populations emerged and proliferated, leading to a scenario where intermediate cells were undetectable by Trp63 and Ck8 immunofluorescence staining in adulthood (data not

shown), and were replaced by fully specialized basal and luminal cells.

2.2. Intermediate cells are potential stem cells

After profiling the identity of intermediate cells by scRNA-seq and histological analyses, we next explored their functional role during prostate development (Fig. 2A). We found that approximately 75% of intermediate cells in neonatal prostate buds highly expressed the cell proliferation marker Ki67 (Fig. 2B and C), aligning with the high proliferation rates detected by scRNA-seq. To assess the proliferative capabilities of intermediate, basal, and luminal cells *in vivo*, we conducted immunostaining for Ki67, the basal cell marker Ck5, and the luminal cell marker Ck8 on prostate sections from 1-week and 2-week-old WT mice. The intermediate cell population ($Ck5^+/Ck8^+$) showed a pronounced Ki67 signal in fluorescence images, and subsequent quantification confirmed that these cells had the highest Ki67 incorporation rates compared to $Ck5^+/Ck8^-$ basal cells and $Ck8^+/Ck5^-$ luminal cells during both early and late postnatal development (Fig. 2D–F).

To directly investigate the function of intermediate cells, we employed enhanced dual recombinases lineage tracing models. We crossed *Trp63-DreER* and *Ck8-CreER* mice with a dual recombinase–activated reporter (*Rosa26-rox-Stop-rox-loxp-Stop-loxp-tdTomato*, termed *R26-Ai66*) to generate the *Trp63-DreER*; *Ck8-CreER*; *R26-Ai66* (TKA) mouse model. The *Trp63-DreER* and *Ck8-CreER* mouse lines have been established to label basal and luminal cells in the mouse prostate, respectively (Guo et al., 2023). Following tamoxifen administration, the Ck8-driven $tdTomato^+$ cells (Cre-*loxp* recombination) were exclusively positive for luminal lineage markers, with about 10% labeling efficiency (Fig. S4A-C), while Trp63-driven $ZsGreen^+$ cells (Dre-*rox* recombination) were strictly basal lineage positive, with labeling efficiency over 90% (Fig. S4D-F). As previously reported (Han et al., 2019), tdTomato activation in *R26-Ai66* reporter model requires both Dre-*rox* and Cre-*loxp* recombination, allowing only the dual-expressing Trp63 and Ck8 cells to be genetically labeled in this TKA model (Fig. 2G).

Next, to evaluate the stemness capacity of intermediate, basal, and luminal cells, we conducted functional *in vitro* organoid formation assay

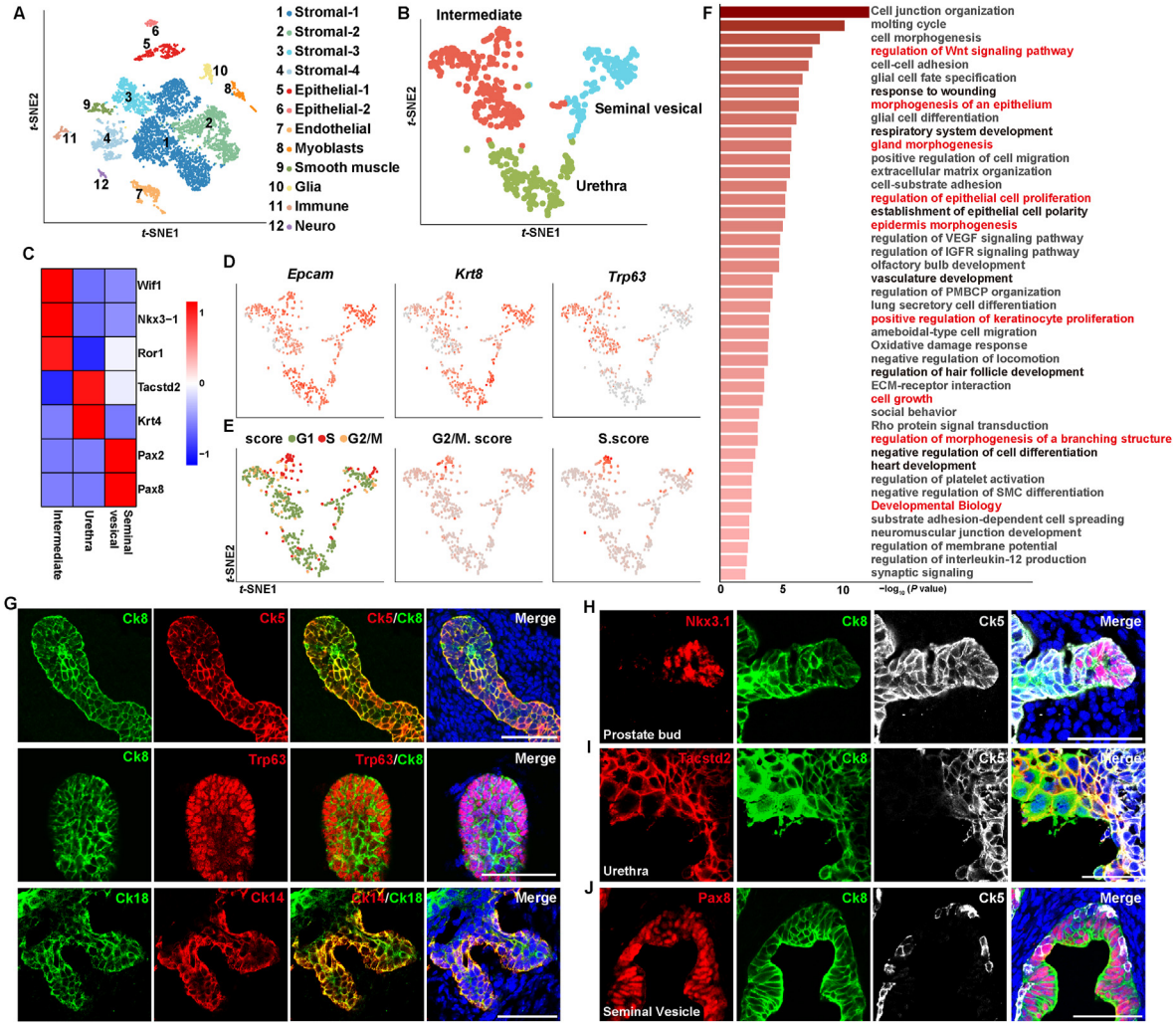

Fig. 1. ScRNA-seq identification of a highly proliferative intermediate cell population. (**A**) Visualization of the clustering of 6868 high quality cells from neonatal mouse urogenital sinus by *t*-SNE. 12 subclusters are identified through unsupervised clustering. (**B**) *t*-SNE visualization of 495 epithelial cells including clusters of Epithelial-1 and Epithelial-2 in (**A**). (**C**) Heatmap of marker gene expression levels in annotated epithelial clusters of intermediate cell, urethra cell and seminal vesicle cell. (**D**) Feature plots showing the gene expression levels of epithelial cell marker *Epcam*, luminal cell marker *Krt8* and basal cell marker *Trp63* across three epithelial cell clusters. (**E**) Feature plots showing the cell cycle phase of epithelial cells and the score of G2/M and S markers. (**F**) Top enriched gene ontology terms based on the differentially expressed genes in intermediate cells compared with urethra and seminal vesicle epithelial cells. (**G**) Co-immunofluorescence of Ck5 and Ck8, Trp63 and Ck8, Ck14 and Ck18 in the prostate buds of WT mice at P0. (**H**) Co-immunofluorescence of Nkx3.1, Ck5 and Ck8 in the prostate buds of WT mice at P0. (**I**) Co-immunofluorescence of Tacstd2, Ck5 and Ck8 in the urethra epithelium of WT mice at P0. (**J**) Co-immunofluorescence of Pax8, Ck5 and Ck8 in the seminal vesicle of WT mice at P0. Scale bars, 50 μm.

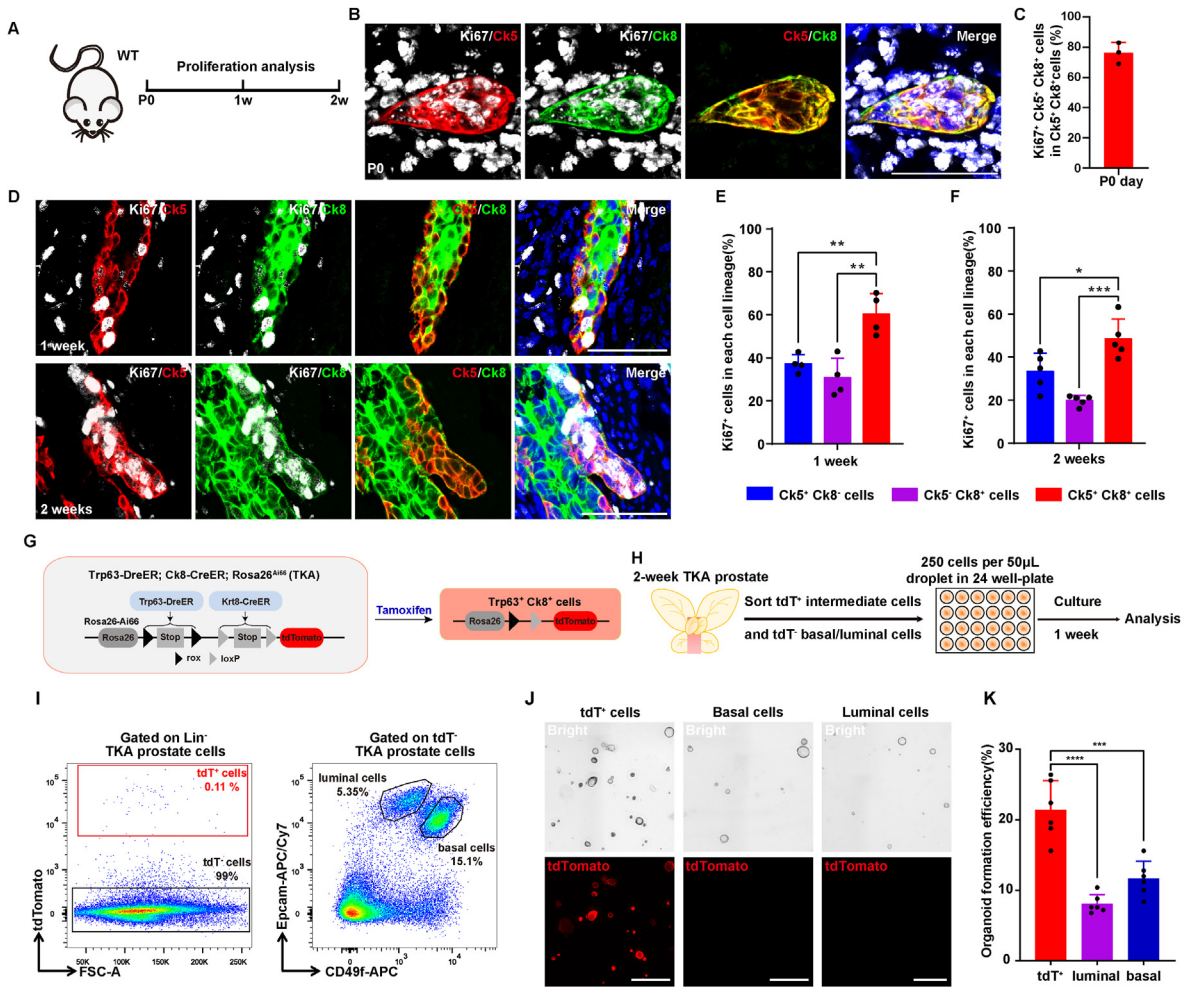

Fig. 2. Intermediate cells are multipotent stem cells *in vitro*. (**A**) Schematic of cell proliferation analysis on basal, luminal and intermediate cells of P0, 1-week- and 2-week-old WT mouse prostates. (**B**) Co-immunofluorescence of Ki67, Ck5 and Ck8 in the prostate buds of P0 day WT mice. (**C**) Percentage of Ki67$^+$ cells among Ck5$^+$/Ck8$^+$ intermediate cells in the prostate buds of WT mice at P0. (**D**) Co-immunofluorescence of Ki67, Ck5 and Ck8 in the prostate of 1-week- and 2-week-old WT mice. (**E, F**) Percentage of Ki67$^+$ cells among Ck5$^+$/Ck8$^+$ intermediate cells, Ck5$^+$/Ck8$^-$ basal cells and Ck8$^+$/Ck5$^-$ luminal cells in the prostate of WT mice at 1 week (**E**) and 2 weeks (**F**) of age. (**G**) Schematic of the targeting strategy to generate TKA mice to label Trp63 and Ck8 co-expressing intermediate cells by tdTomato expression. (**H**) Timeline of sorting and organoid culture of tdTomato$^+$ intermediate cells, tdTomato$^-$ basal and luminal cells from 2-week-old TKA prostates. (**I**) FACS plot showing tdTomato$^+$ intermediate cells isolated from Lin$^-$ prostate single cells, tdTomato$^-$ basal and luminal cells isolated from the epithelial cells (Epcam^{high}) of 2-week-old TKA mouse prostates. (**J**) Micrographs of organoids formed by tdTomato$^+$ intermediate cells, tdTomato$^-$ basal and luminal cells. Scale bar, 1 mm. (**K**) Organoid formation efficiency of tdTomato$^+$ intermediate cells, tdTomato$^-$ basal and luminal cells calculated after 1 week of culture. Scale bars, 50 μm. Data are shown as the mean ± SD. Data were analyzed by One-way ANOVA; *$p < 0.05$, **$p < 0.01$, ***$p < 0.001$ and ****$p < 0.0001$.

(Fig. 2H). Using the enhanced dual recombinase TKA mouse model, we isolated tdTomato$^+$ intermediate cells (tdTomato$^+$/Lin$^-$), tdTomato$^-$ basal cells (tdTomato$^-$/Lin$^-$/Epcam^{high}/CD49f^{high}), and tdTomato$^-$ luminal cells (tdTomato$^-$/Lin$^-$/Epcam^{high}/CD49f^{med}) by fluorescence-activated cell sorting (FACS) two days post-tamoxifen induction in 2-week-old TKA mice (Fig. 2I and Fig. S5A). The organoid-forming efficiency was then compared (Drost et al., 2016). Notably, tdTomato$^+$ intermediate cells exhibited significantly higher organoid-forming ability than both the tdTomato$^-$ basal cells and luminal cells (Fig. 2J and K). The organoids derived from tdTomato$^+$ intermediate cells maintained tdTomato signal and expressed both basal (Trp63/Ck5) and luminal (Ck8) markers (Fig. S5B), reinforcing the notion of intermediate cells as a viable stem cell population.

2.3. Lineage tracing of intermediate cells during prostate development

We further explored the cellular dynamics of intermediate cells *in vivo* using TKA mouse model during both early and late stages of prostate development. To examinate the cellular identity of tdTomato-labeled Trp63$^+$/Ck8$^+$ intermediate cells, TKA mice at various developmental stages, postnatal day 0 (P0), 1-week and 2-week-old, were treated with tamoxifen. Prostate tissues were then collected two days after tamoxifen administration for further analysis. Immunostaining for Trp63 and Ck8 on prostate sections from the above three stages confirmed that all tdTomato$^+$ cells were double-positive for Trp63 and Ck8 (Fig. 3A–C). There was no tdTomato expression Trp63$^+$/Ck8$^-$ basal cells or in Ck8$^+$/Trp63$^-$ luminal cells. The proportion of tdTomato$^+$ intermediate cells was about 25% of the epithelial cells in neonatal TKA mouse prostate, but this ratio decreased over time, reflecting a rapidly reduction in the intermediate cell population during prostate postnatal development (Fig. 3D and E). All these results confirmed that only Trp63 and Ck8 co-expressing intermediate cells were genetically labeled in TKA mice (Fig. 3F).

To determine the cell fate of these tdTomato$^+$ intermediate cells *in vivo*, we conducted lineage tracing assays and analyzed prostate tissues from 8 weeks-old adult TKA mice, when tamoxifen was administrated at P0, postnatal day 7 (P7) and day 14 (P14). Immunostaining for Trp63 and Ck8 showed that tdTomato$^+$ intermediate cells labeled at P0 were capable of generating both basal and luminal cells (Fig. 3G).

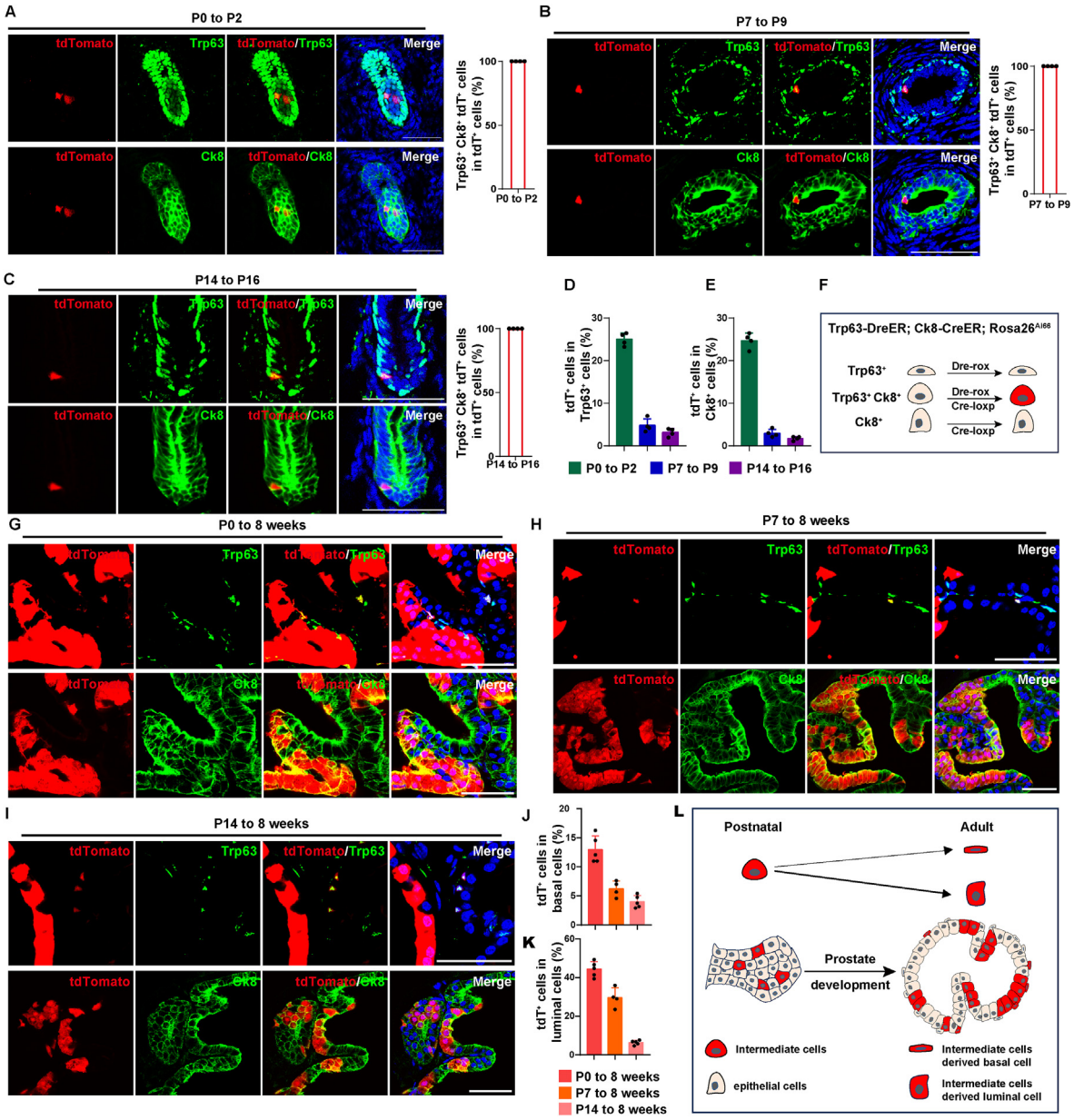

Fig. 3. Intrinsic bipotent intermediate stem cells during the prostate development. (**A-C**) Co-immunofluorescence of Trp63 and Ck8 with endogenous tdTomato in the P0 (**A**), 1-week-old (**B**), and 2-week-old (**C**) prostates of the TKA mice 2 days after tamoxifen injection. Percentage of Trp63$^+$/Ck8$^+$/tdTomato$^+$ cells among tdTomato$^+$ intermediate cells in P0 (**A**), 1-week-old (**B**), and 2-week-old (**C**) prostates of TKA mice. (**D, E**) Percentage of tdTomato$^+$ cells in Trp63$^+$ basal cells (**D**) and Ck8$^+$ luminal cells (**E**) of TKA mouse prostates 2 days after tamoxifen administration at P0, 1 week and 2 weeks of age. (**F**) Schematic of the labeling of Trp63$^+$/Ck8$^+$ intermediate cells with tdTomato signal in TKA mice. (**G-I**) Immunostaining for Trp63 and Ck8 in the adult TKA mouse prostate sections treated with tamoxifen at P0 (**G**), 1-week-old (**H**), and 2-week-old (**I**). (**J, K**) Percentage of tdTomato$^+$ daughter cells in Trp63$^+$ basal cells (**J**) and Ck8$^+$ luminal cells (**K**) of adult TKA mice treated with tamoxifen at P0, 1 week and 2 weeks of age. (**L**) Schematic diagram suggesting that intrinsic bipotent intermediate cells serve as prostate stem cells in prostate development. Scale bars, 50 μm. Data are shown as the mean ± SD.

Furthermore, these bipotent tdTomato$^+$ intermediate cells persisted at early and late postnatal stages, generating both basal and luminal progeny (Fig. 3H and I). Quantitative analysis showed that tdTomato$^+$ basal daughter cells, originating from intermediate cells labeled at P0, P7, and P14, accounted for approximately 13.00% ± 2.34%, 6.22% ± 1.37%, and 4.01% ± 1.06% of Trp63$^+$ basal cells in anterior prostate lobes, respectively (Fig. 3J). It was also observed that tdTomato$^+$ intermediate cells tended to predominantly form luminal cells, with their luminal progeny constituting about 44.47% ± 4.01%, 29.59% ± 5.09%, and 6.37% ± 1.15% of Ck8$^+$ luminal cells in anterior prostate lobes, respectively (Fig. 3K).

Considering the heterogeneity among different lobes of the mouse prostate, we also traced the lineage and composition of tdTomato$^+$ intermediate daughter cells in both the dorsolateral lobes (DLP) and ventral lobes (VP), where similar bipotent potential was observed (Fig. S6A-J). These results demonstrated that tdTomato$^+$ intermediate cells maintain intrinsic bipotential properties throughout early stages of prostate development, giving rise to both basal and luminal daughter cells (Fig. 3L).

2.4. Intermediate cell is bipotent stem cell during prostate postnatal development

To explore the lineage plasticity and proliferative capabilities of

intermediate cells, we utilized the dual recombinase-activated reporter *R26*-TLR (*Rosa26*-CAG-*rox-stop-rox-ZsGreen-Insulater-CAG-loxp-stop-loxp-tdTomato*) mouse model (Liu et al., 2020). By generating the *Trp63-DreER*; *Ck8-CreER*; *R26*-TLR (TK-TLR) mouse, we were able to distinctly label Trp63$^+$ basal cells as ZsGreen$^+$ cells (via Dre-*rox* recombination), Ck8$^+$ luminal cells as tdTomato$^+$ cells (via Cre-*loxp* recombination), and Trp63$^+$/Ck8$^+$ double-positive intermediate cells as ZsGreen$^+$/tdTomato$^+$ cells (via both Dre-*rox* and Cre-*loxp* recombination) (Fig. 4A). This TK-TLR model allows for the simultaneously genetic tracing of the cell lineage dynamics of these three cell types.

Two days after tamoxifen administration at early (P7) and late (P14) postnatal stages, prostate tissues were harvested for analysis (Fig. 4B). Immunofluorescence confirmed that ZsGreen$^+$/tdTomato$^+$ intermediate cells consistently expressed both the basal marker Trp63 and luminal marker Ck8 at both developmental stages (Fig. 4C–E), thus validating the specific tracing of intermediate cells in the TK-TLR model (Fig. 4G).

Further investigations into the cell fate and organogenesis capacity of ZsGreen$^+$/tdTomato$^+$ intermediate cells were conducted from early and late development stages to adulthood (Fig. 4B). Immunostaining of prostate sections for Trp63 and Ck8 revealed that ZsGreen$^+$/tdTomato$^+$

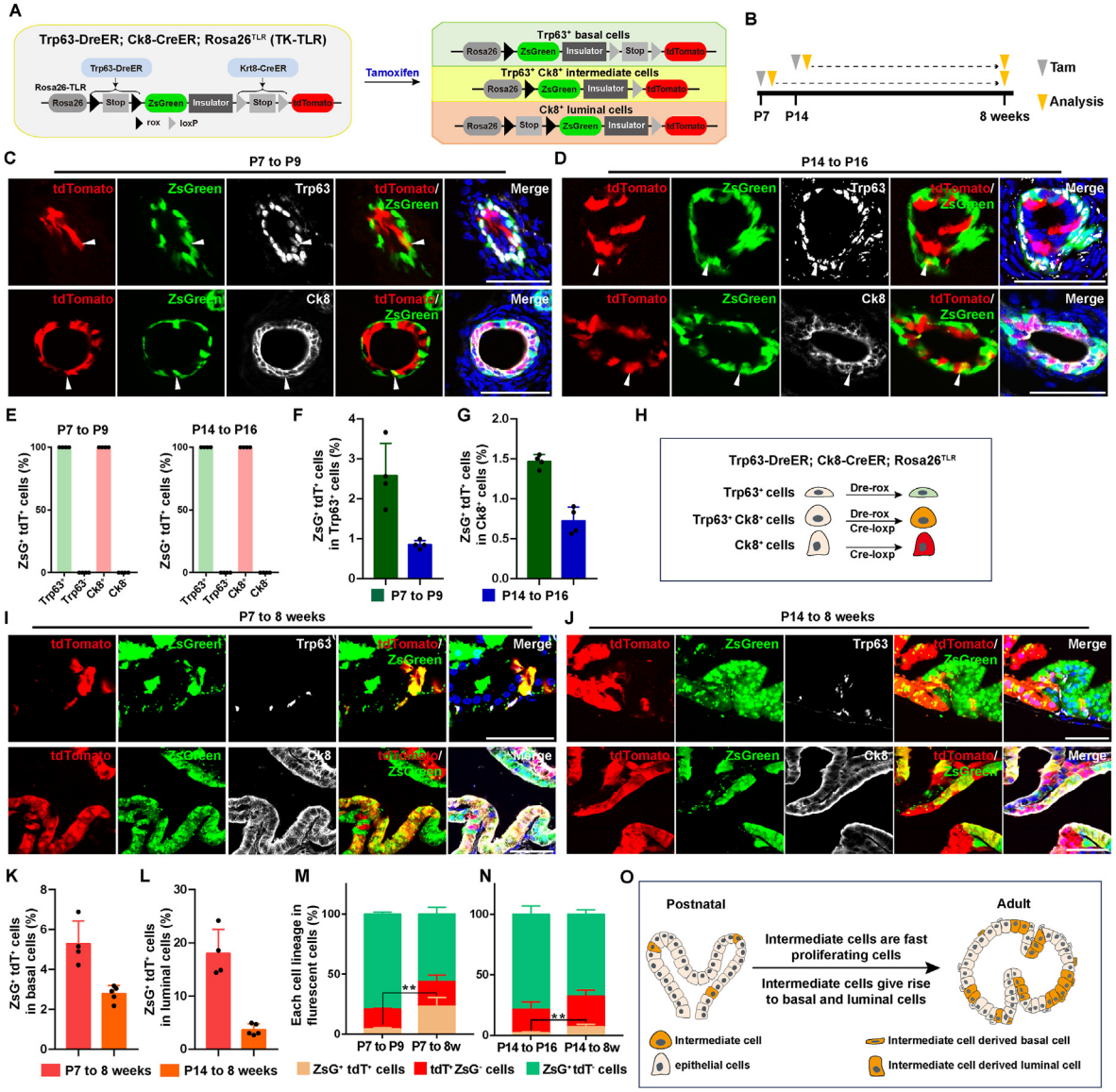

Fig. 4. Simultaneous tracing of diverse prostate epithelial cells. (**A**) Schematic diagram of targeting strategy for simultaneous labeling of Trp63$^+$ cells, Ck8$^+$ cells and Trp63 and Ck8 co-expressing intermediate cells using TK-TLR mouse model. (**B**) Timeline of tamoxifen administration and TK-TLR mouse prostate analysis time. Tam is short for tamoxifen injection. (**C, D**) Immunostaining for Trp63 and Ck8 in 1-week-old (**C**) and 2-week-old (**D**) prostates of TK-TLR mice 2 days after tamoxifen injection. White arrows indicate intermediate cells (ZsGreen$^+$/tdTomato$^+$). (**E**) Percentage of ZsGreen$^+$/tdTomato$^+$ intermediate cells among Trp63$^+$ cells and Trp63$^-$ cells, Ck8$^+$ cells and Ck8$^-$ cells in 1 week and 2 weeks old TK-TLR mice 2 days after tamoxifen treatment. (**F, G**) Percentage of ZsGreen$^+$/tdTomato$^+$ intermediate cells among Trp63$^+$ basal cells (**F**) and Ck8$^+$ luminal cells (**G**) of TK-TLR mice 2 days after tamoxifen administration at 1 week and 2 weeks of age. (**H**) Schematic diagram of labeling of Trp63$^+$ Ck8$^+$ intermediate cells with ZsGreen and tdTomato signal in TK-TLR mice. (**I, J**) Immunostaining for Trp63 and Ck8 in the adult TK-TLR mouse prostate sections treated with tamoxifen at 1-week-old (**I**), and 2-week-old (**J**). (**K, L**) Percentage of ZsGreen$^+$/tdTomato$^+$ daughter cells in Trp63$^+$ basal cells (**K**) and Ck8$^+$ luminal cells (**L**) of adult TK-TLR mice treated with tamoxifen at 1 week and 2 weeks of age. (**M, N**) Percentage of ZsGreen$^+$/tdTomato$^+$ cells, ZsGreen$^+$/tdTomato$^-$ cells and tdTomato$^+$/ZsGreen$^-$ cells among all fluorescent cells in prostate tissues of P9 and 8-week TK-TLR mice injected with tamoxifen at 1 week of age (**M**), and in prostate tissue of P16 and 8-week TK-TLR mice injected with tamoxifen at 2 weeks of age (**N**). (**O**) Schematic diagram suggesting that intermediate cells are rapidly proliferating bipotent prostate stem cells in prostate development. Scale bars, 50 μm. Data are shown as the mean ± SD. Data were analyzed by unpaired two-tailed Student's *t*-test; $^{**}p < 0.01$.

intermediate cells derived from early postnatal stage were capable of giving rise to both basal and luminal cells, demonstrating their bipotent plasticity (Fig. 4I). This bipotent lineage was consistently observed from P14 to 8 weeks, indicating a stable bipotent lineage differentiation capacity over time (Fig. 4J). Contributions of these cells to both basal and luminal cell populations were also confirmed in different lobes such as DLP and VP (Fig. S7A-H).

To quantify the proliferative capacity of intermediate cells, we noted that ZsGreen$^+$/tdTomato$^+$ intermediate cells constituted only a small fraction of the Trp63$^+$ cells at P7 (2.58% ± 0.81%) and P14 (0.85% ± 0.10%), but their presence significantly increased to 5.30% ± 1.13% and 2.80% ± 0.40% in basal cells of adult anterior prostate lobes (Fig. 4F–K). Similarly, the proportion of these ZsGreen$^+$/tdTomato$^+$ intermediate cells within the Ck8$^+$ luminal cells also showed a marked increase from P7 and P14 to 8 weeks (from 1.47% ± 0.09% to 18.00% ± 4.52% at P7, and from 0.72% ± 0.09% to 3.69% ± 1.06% at P14) (Fig. 4G–L).

By accounting for all fluorescent cells, including both single and double positive cells, we quantified the ratio of ZsGreen$^+$/tdTomato$^+$ intermediate cells from the tracing start points (P7 and P14) to the tracing end point (8 weeks). This quantification revealed a significant increase in the proportion of ZsGreen$^+$/tdTomato$^+$ intermediate cells, highlighting their substantial contribution to prostate organogenesis (Fig. 4K-N). This data underscores the considerable proliferative and developmental impact of these bipotent intermediate cells within the prostate gland.

2.5. Neuroendocrine cell transformation during prostate development

The phenomenon of drug resistance in prostate cancer therapy is often linked to the cell lineage plasticity of luminal cancer cell to neuroendocrine cell differentiation (Davies et al., 2018). To investigate the presence and characteristics of neuroendocrine cells during prostate organogenesis, we conducted immunofluorescence staining for the neuroendocrine marker Chromogranin A (Chga) in neonatal prostate cells. We observed Chga-expressing cells as early as P0 in prostate buds. Notably, most neonatal Chga-expressing cells were found to co-express both Ck5 and Ck8, indicating their possession of neuroendocrine, basal, and luminal triple-positive cell feature (Fig. 5A–E). Further immunostaining for neuroendocrine, basal and luminal markers was performed on prostate sections from 1-week-old to 8-week-old mice. We observed a marked loss of basal cell features in Chga-expressing cells at 1-week-old and 2-week-old stages, although these cells continued to express the luminal cell marker. During early postnatal development, 13.8% ± 3.1% of Chga-expressing cells maintained co-expressing of Ck5 and Ck8, whereas in late postnatal development, 6.4% ± 1.0% of Chga$^+$ cells maintained this co-expression (Fig. 5B, C, E and Fig. S8A, B). In adult prostate tissues, Chga-expressing neuroendocrine cells had completely lost basal cell marker Ck5 expression and only expressed the luminal cell marker Ck8 (Fig. 5D and E).

To further explore the neuroendocrine characteristics in intermediate cells, we utilized our enhanced dual recombinases system in the TKA mouse model. In neonatal TKA mouse prostates, 14.2% ± 2.2% of Chga-expressing cells were identified as tdTomato$^+$ intermediate cells (Fig. 5F and G). Among these, 12.6% ± 2.5% of Chga$^+$ neuroendocrine cells maintained tdTomato expression into adulthood, and these Chga$^+$/tdTomato$^+$ daughter cells lacked expression of Ck5, aligning with the expression of luminal cell marker Ck8 (Fig. 5H and I). Furthermore, in neonatal TK-TLR mouse prostates, 11.3% ± 0.7% of Chga-expressing cells were ZsGreen$^+$/tdTomato$^+$ intermediate cells. In the adult TK-TLR mouse model, 10.4% ± 3.3% of Chga$^+$ neuroendocrine cells continued to co-express ZsGreen and tdTomato (Fig. 5J and K).

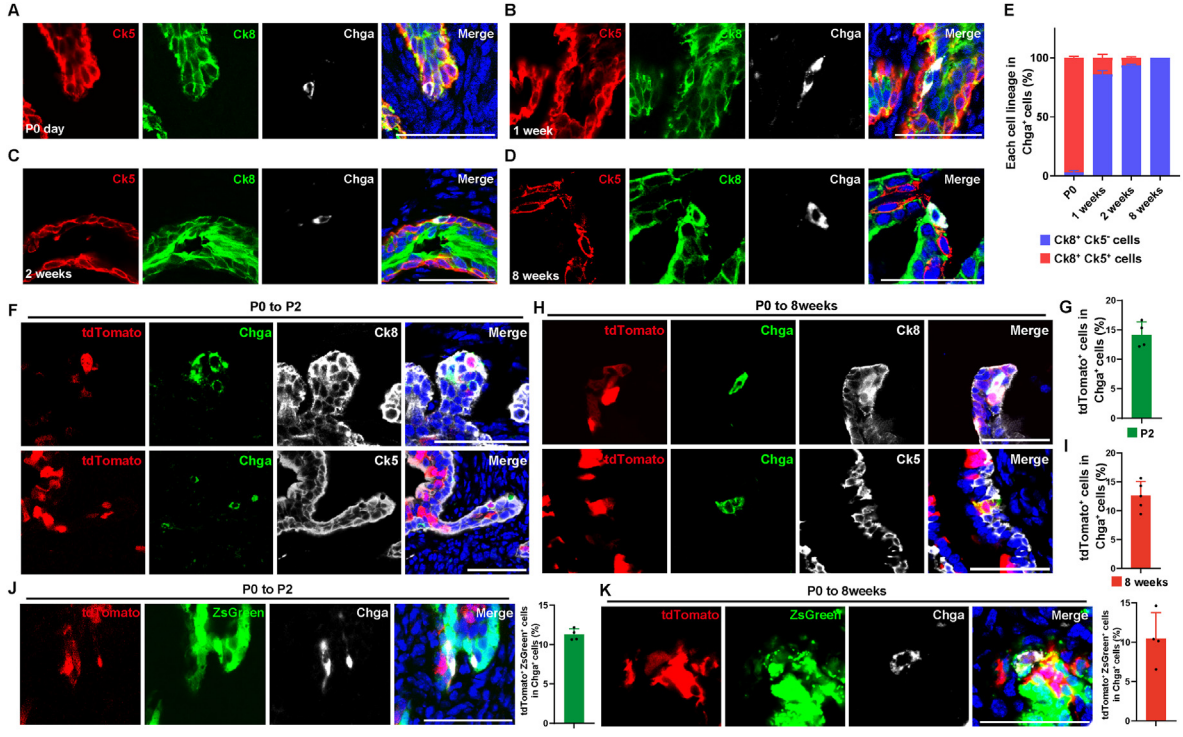

Fig. 5. Neuroendocrine cell marker-expressing cell transformation during prostate development. (**A-D**) Co-immunofluorescence of Chga, Ck5 and Ck8 in the prostate tissues of P0 (**A**), 1-week-old (**B**), 2-week-old (**C**) and 8-week-old (**D**) WT mice. (**E**) Bar graph showing the percentage of Chga$^+$/Ck5$^+$/Ck8$^+$ cells and Chga$^+$/Ck5$^-$/Ck8$^+$ cells among Chga$^+$ cells of WT mouse prostates at P0, 1 week, 2 weeks and 8 weeks of age. (**F** and **H**) Co-immunofluorescence of Chga, Ck5 and Ck8 with endogenous tdTomato in P2 prostate buds (**F**), and adult prostates (**H**) of TKA mice treated with tamoxifen at P0. (**G** and **I**) Bar graphs showing the percentage of tdTomato$^+$/Chga$^+$ cells among Chga$^+$ cells of TKA mouse prostates at P2 (**G**) and 8 weeks (**I**). (**J** and **K**) Immunostaining for Chga, endogenous tdTomato and ZsGreen in the P2 prostate buds (**J**), and in the adult prostates (**K**) of TK-TLR mice that were treated with tamoxifen at P0, bar graphs showing the percentage of tdTomato$^+$/ZsGreen$^+$/Chga$^+$ cells among Chga$^+$ cells of TK-TLR mouse prostates at P2 (**J**) and 8 weeks (**K**). Data are shown as the mean ± SD. Scale bars, 50 μm.

Taken together, these findings suggest a cell lineage transition from triple-positive (basal, luminal, and neuroendocrine) cells to double-positive (luminal and neuroendocrine) cells. This transition may provide valuable insights into the neuroendocrine lineage plasticity and its implications in the progression of prostate cancer cells, potentially influencing therapeutic strategies targeting neuroendocrine differentiation in prostate cancer.

3. Discussion

Organogenesis, tissue regeneration, and cancer progression are fundamentally influenced by the proliferation and lineage transformation of tissue-specific stem cells (Blanpain & Simons, 2013). In this study, we have advanced the understanding of these processes by generating a scRNA-seq profile of neonatal mouse prostate cells. This profiling effort has enabled us to define cell identities and delineate a unique population of intermediate cell endowed with stem cell potential. By employing enhanced lineage tracing strategies in both *in vitro* organoid formation (Fu et al., 2021; Gao et al., 2014; Karthaus et al., 2014) and *in vivo* cell fate mapping assays, we have demonstrated that these intermediate cells possess substantial proliferative capacity and exhibit bipotency during prostate development. This finding is crucial as the transition from prostate adenocarcinoma to NEPC contributes to resistance against androgen-deprivation therapy. Our results not only confirmed the existence of neuroendocrine cells in the neonatal prostate, but also clarify the epithelial lineage transition of these cells, providing deep insights into the onset and progression of NEPC.

Historically, lineage plasticity and developmental trajectories in prostate development were explored using single-marker-driven lineage tracing techniques. However, the precision of such methods hinges on the accurate expression of Cre recombinase, controlled by cell lineage-specific promoter (Davis et al., 2012; He et al., 2017). Single promoter-driven recombinase strategies often result in labeling biases and fail to comprehensively capture the fate of multi-lineage cells. The enhanced lineage tracing assays overcome these limitations by specifically mapping intermediate cells during prostate development (He et al., 2017). We propose a model of prostate development wherein intermediate cells are identified as bipotent stem cells that maintain their bipotency throughout postnatal development.

The current lineage tracing models have technical limitations. Specifically, it is challenging to distinctly identify the fate of each intermediate cell at the single-cell level throughout the development of the prostate. Recent advancements in lineage tracing assays now enable the tracking of single-cell clones by recording clonal information using DNA sequence barcodes (Wagner & Klein, 2020). Nevertheless, the effectiveness of the enhanced dual recombinase mouse systems is dependent on tamoxifen, which requires time to act, whereas prostate development occurs very rapidly. Integrating more advanced sequencing techniques with innovative lineage tracing methods could yield a comprehensive understanding of intermediate cells and offer valuable insights into developmental biology and disease mechanisms.

Recent research, including our own, has highlighted the significant role of intermediate cells in various contexts such as bacteria-induced prostate inflammation, benign prostatic hyperplasia (BPH), and ERG-driven invasive prostate cancer (Feng et al., 2023; Guo et al., 2023). The parallels between prostate cancer cells and prostate development, particularly the reactivation of developmental patterns during tumorigenesis, underscore the importance of studying stem cells within prostate biology (Toivanen & Shen, 2017).

The relevance of intermediate cells extends beyond prostate biology. Their pivotal roles have been identified in various tissues, including both glandular and non-glandular epithelia tissues, under different pathological conditions (Ma et al., 2022; Pu et al., 2023; Wuidart et al., 2018). These findings emphasize the necessity of understanding the properties and lineage plasticity of intermediate cells in the broader contexts of development, regeneration, and disease progression.

Our study not only sheds light on the characteristics and function of intermediate cells, but also provides fundamental insights into development and disease progression associated with intermediate stem cells. This knowledge base could pave the way for novel therapeutic strategies targeting stem cell dynamics in prostate disease and potentially other related conditions.

4. Materials and methods

Mice. All experimental mouse studies were conducted in accordance with recent guidelines of the Animal Care and Use Committee at the Center of Excellence in Molecular Cell Science, Chinese Academy of Sciences (CAS). All experimental mice were fed and kept according to rules in accordance with the regulations of the Shanghai Laboratory Animal Center Institutional Animal. *Rosa26-loxp-stop-loxp-EYFP* (Srinivas et al., 2001), *Rosa26-loxp-stop-loxp-tdTomato* (Madisen et al., 2010) and *Rosa26-CreER* mice were purchased from the Jackson Laboratory. As published previously (Han et al., 2019, 2021; He et al., 2021; Liu et al., 2020), *Rosa26*-TLR, *Rosa26-Ai66*, *and Trp63-DreER* mouse lines were provided by Bin Zhou. *Ck8-CreER* mice were provided by Li Xin (Zhang et al., 2012).

Genomic PCR. Experimental mice were genotyped by PCR using the genomic DNA obtained from mouse tail. Each mouse tail tissue was lysed by incubation with 500 μL lysis buffer (50 mM Tris-HCl, pH8; 100 mM EDTA; 100 mM NaCl; 1% SDS; 0.5 mg/mL Proteinase K) for 2 h at 55 °C with shaking, and added with 250 μL saturated NaCl, and the mixture was centrifuged at 12000 rpm for 10 min to obtain a supernatant containing genomic DNA. Genomic DNA was precipitated with isopropanol, washed with 70% ethanol and dissolved in deionized water. The sequences of the genotyping primers specific for each mouse line and the expected band sizes for PCR, are listed in Supplementary Table 1.

Mouse lineage tracing procedures. For newborn mice, tamoxifen (Sigma, cat. no. T6648-5G, 20 mg/mL dissolved in corn oil) was administrated by subcutaneous injection under the back skin. For 1-week-old, 2-week-old and adult mice, tamoxifen was administrated by intragastric injection.

Prostate cell dissociation and sorting. Mice were euthanized using carbon dioxide asphyxiation, and the urogenital tract was removed and placed in cold PBS. The seminal vesicles, vas deferens, bladder, urethra, and adipose tissue were removed from the urogenital tract under a stereomicroscope to isolate the prostate tissue. Mouse prostate tissue was dissected and cut into small pieces under a microscope, followed by enzymatic dissociation with 0.5 mL of dissociation medium (1 × Collagenase/Hyaluronidase, STEMCELL, no. 07912) for 30 min at 37 °C with shaking. The dissociated tissue chunks were spun down at 800 rpm for 1 min, and then the supernatant was removed. The dissociated tissue chunks were further dissociated by TrypLE (Gibco, no.12605-028) with 10 μm Y27632 for 10 min at 37 °C. The dissociated prostate cells were stained with directly conjugated primary antibodies (Supplementary Table 2) for 30 min on ice. The dissociated cell suspension was filtered through a 45 μm mesh filter. Cells were sorted on a FACS Aria II (BD).

Organoid formation assay. We used a previously published protocol to perform the prostate organoid formation assay (Drost et al., 2016; Guo et al., 2020). Briefly, sorted mouse prostate cells were suspended in the mouse prostate organoid medium (Drost et al., 2016) and an equal volume of Matrigel (Corning 354234) was added. The cell suspension was placed into a 24-well culture plate (Corning) at a concentration of 250 cells per 50 μL droplet. After incubated in a cell incubator (5% CO_2, 37 °C) for 30 min, mouse prostate organoid medium was added to the cell culture plates, and medium was replenished every 3 days. The organoids were cultured for 7 days, and for statistical analysis, the microscope images were taken with Cytation 5, and organoid measurements and statistics were processed by Gen 5 Image Prime.

Tissue embedding and immunostaining assay. Experimental mice were euthanized and prostate tissues were micro-dissected under a

stereoscope. Prostate tissues were fixed in 4% paraformaldehyde for 2 h at 4 °C. After being washed three times in 4 °C PBS, prostate tissues were dehydrated in cold 30% sucrose overnight, then embedded in OCT compound. Organoids were fixed with 4% paraformaldehyde for 30 min at 4 °C, and washed three times in cold PBS. Organoids were dehydrated in 30% sucrose for 2 h at 4 °C, then embedded in OCT compound. The frozen tissues and organoids were stored at −80 °C. Cryosections (~10 μm) were collected on adhesive microscope slides and stored at −20 °C until use.

The dried sections were washed three times with PBS, then were permeabilized and blocked with 5% goat serum in PBST (0.1% Triton X-100 in PBS). Sections were stained with primary antibodies in 5% goat serum overnight at 4 °C, then washed three times with PBST (0.05% Tween-20 in PBS) and incubated with secondary antibodies for 1 h at room temperature in the dark. Sections were then washed three times with PBST (0.05% Tween-20 in PBS) and mounted with DAPI (Sigma). Primary and secondary antibodies are listed in Supplementary Table 2. Immunofluorescence images were captured using a Leika (sted) confocal system. Images were analyzed using Image J software.

Prostate cell digestion and scRNA-seq library construction. The urogenital tissues with prostate buds from neonatal mice were sectioned under a stereomicroscope, followed by enzymatic dissociation with 0.5 mL of 1% Trypsin for 30 min at 4 °C. The dissociated tissues were washed with DMEM twice, and further dissociated by 0.1% collagenase B, with 1% DNase for 15 min at 37 °C. After quenched by DMEM with 10% FBS, the urogenital tract cells were passed through a 45 μm filter. For scRNA-seq, the dead cells were removed from urogenital tract cells by Dead cell removal kit (Miltenyi, 130-090-101). And the 13,800 live urogenital tract cells were loaded in a Single-Cell-G-Chip. The Single-Cell-A-Chip with live urogenital tract cells was loaded on a 10X Chromium single-cell instrument (10X Genomics). According to the manufacturer's instructions, we conducted barcoding, complementary DNA synthesis and library construction. The live urogenital tract cell sample was run on a NovaSeq6000 (Illumina).

Single-cell RNA-seq data preprocessing. Raw sequencing data was preprocessed by Cell Ranger (version 7.1.0) and reads were mapped against the mm10 mouse reference genome. Filtered gene expression matrix was used to create seurat object in R (version 4.3.1) with the package of Seurat (version 4.4.0). Quality control was performed with the criterion of more than 200 detected genes and less than 20% mitochondrial gene ratio. Standard preprocessing workflow with default parameters was applied for single-cell RNA data including the function of NormalizeData, FindVariableFeatures, ScaleData and RunPCA. Following the clustering cells by the function of FindNeighbors and FindClusters with parameters of 50 dimensions and 0.3 resolutions separately, non-linear dimensional reduction was performed using RunTSNE with parameters of 50 dimensions. Cluster 10 was removed because there were low-quality cells with generally lower number of genes and counts. After quality control, 7210 high-quality cells were identified and standard processing workflow was applied once more as described above. Differently, parameters were 18 dimensions and 0.085 resolutions in the step of clustering cells. Subsequently, differentially expressed genes for each cluster were identified by the function of FindAllMarkers, and clusters were annotated according to the specific cell markers.

Cell cycle heterogeneity analysis of epithelial cells. Cell cycle state was assessed based on the expression of G2/M and S phase markers which are stored in a list named cc.genes in the package of Seurat (version 4.4.0). Cell cycle phase scores were calculated by the function of CellCycleScoring.

Gene Ontology and pathway enrichment analyses. Top 150 most highly differentially expressed genes of intermediate cells among epithelial cells which were identified by the function of FindAllMarkers, were applied to enrich pathway using Metascape and enriched pathway (p-value <0.01) were presented.

Quantification and statistics. At least three replications were performed to organoid formation assays, and at least three mice were used for lineage tracing, library construction and organoid formation assays. We analyzed at least 5 sections for immunofluorescent staining.

Data and materials availability. The raw sequencing data for the scRNA-seq of urogenital sinus of neonatal mice have been deposited in the Gene Expression Omnibus (GEO; https://www.ncbi.nlm.nih.gov/geo) with the accession number GSE270830, https://www.ncbi.nlm.nih.gov/geo/query/acc.cgi?&acc=GSE270830.

CRediT authorship contribution statement

Xiaoyu Zhang: Writing – original draft, Validation, Investigation, Data curation. **Jian Wang:** Validation, Software. **Wangxin Guo:** Validation, Investigation. **Hongjiong Zhang:** Validation. **Bin Zhou:** Resources. **Chen Yu:** Resources. **Dong Gao:** Writing – review & editing, Project administration, Funding acquisition, Conceptualization.

Declaration of competing interest

The authors have no competing interests to declare.

Acknowledgements

We thank Baojin Wu, Guoyuan Chen and Wei Bian for providing technical help at the CEMCS (SIBCB) Core Facility, and the Genome Tagging Project (GTP) Center at CEMCS for technical support. This study was supported by the National Key Research and Development Program of China (No. 2020YFA0509002, 2023YFC2506401), the National Science Fund for Distinguished Young Scholars (32125013), the National Natural Science Foundation of China (92253304), the Basic Frontier Science Research Program of Chinese Academy of Sciences (ZDBS-LY-SM015), the Shanghai Science and Technology Committee (21XD1424200 and 21ZR1470100), the Shanghai Municipal Science and Technology Major Project and the Innovative Research Team of High-level Local Universities in Shanghai (SHSMUZDCX20211800).

Appendix A. Supplementary data

Supplementary data to this article can be found online at https://doi.org/10.1016/j.cellin.2024.100182.

References

Bhatia-Gaur, R., Donjacour, A. A., Sciavolino, P. J., Kim, M., Desai, N., Young, P., Norton, C. R., Gridley, T., Cardiff, R. D., Cunha, G. R., et al. (1999). Roles for Nkx3.1 in prostate development and cancer. *Genes Dev, 13*, 966–977.

Blanpain, C., & Simons, B. D. (2013). Unravelling stem cell dynamics by lineage tracing. *Nature Reviews Molecular Cell Biology, 14*, 489–502.

Centonze, A., Lin, S., Tika, E., Sifrim, A., Fioramonti, M., Malfait, M., Song, Y., Wuidart, A., Van Herck, J., Dannau, A., et al. (2020). Heterotypic cell-cell communication regulates glandular stem cell multipotency. *Nature, 584*, 608–613.

Chan, J. M., Zaidi, S., Love, J. R., Zhao, J. L., Setty, M., Wadosky, K. M., Gopalan, A., Choo, Z. N., Persad, S., Choi, J., et al. (2022). Lineage plasticity in prostate cancer depends on JAK/STAT inflammatory signaling. *Science, 377*, 1180–1191.

Chen, S., Zhu, G., Yang, Y., Wang, F., Xiao, Y. T., Zhang, N., Bian, X., Zhu, Y., Yu, Y., Liu, F., et al. (2021). Single-cell analysis reveals transcriptomic remodellings in distinct cell types that contribute to human prostate cancer progression. *Nature Cell Biology, 23*, 87–98.

Choi, N., Zhang, B., Zhang, L., Ittmann, M., & Xin, L. (2012). Adult murine prostate basal and luminal cells are self-sustained lineages that can both serve as targets for prostate cancer initiation. *Cancer Cell, 21*, 253–265.

Davies, A. H., Beltran, H., & Zoubeidi, A. (2018). Cellular plasticity and the neuroendocrine phenotype in prostate cancer. *Nature Reviews Urology, 15*, 271–286.

Davis, J., Maillet, M., Miano, J. M., & Molkentin, J. D. (2012). Lost in transgenesis: A user's guide for genetically manipulating the mouse in cardiac research. *Circulation Research, 111*, 761–777.

Deng, S., Wang, C., Wang, Y., Xu, Y., Li, X., Johnson, N. A., Mukherji, A., Lo, U. G., Xu, L., Gonzalez, J., et al. (2022). Ectopic JAK-STAT activation enables the transition to a stem-like and multilineage state conferring AR-targeted therapy resistance. *Nature Canada, 3*, 1071–1087.

Drost, J., Karthaus, W. R., Gao, D., Driehuis, E., Sawyers, C. L., Chen, Y., & Clevers, H. (2016). Organoid culture systems for prostate epithelial and cancer tissue. *Nature Protocols, 11*, 347–358.

Feng, W., Ladewig, E., Salsabeel, N., Zhao, H., Lee, Y. S., Gopalan, A., Luo, H., Kang, W., Fan, N., Rosiek, E., et al. (2023). *ERG-driven prostate cancer emerges from basal-luminal hybrid cells*, Article 540839, 2023.2005.2015.

Fu, X., He, Q., Tao, Y., Wang, M., Wang, W., Wang, Y., Yu, Q. C., Zhang, F., Zhang, X., Chen, Y. G., et al. (2021). Recent advances in tissue stem cells. *Science China Life Sciences, 64*, 1998–2029.

Gao, D., Vela, I., Sboner, A., Iaquinta, P. J., Karthaus, W. R., Gopalan, A., Dowling, C., Wanjala, J. N., Undvall, E. A., Arora, V. K., et al. (2014). Organoid cultures derived from patients with advanced prostate cancer. *Cell, 159*, 176–187.

Germanos, A. A., Arora, S., Zheng, Y., Goddard, E. T., Coleman, I. M., Ku, A. T., Wilkinson, S., Song, H., Brady, N. J., Amezquita, R. A., et al. (2022). Defining cellular population dynamics at single-cell resolution during prostate cancer progression. *Elife, 11*.

Guo, W., Li, L., He, J., Liu, Z., Han, M., Li, F., Xia, X., Zhang, X., Zhu, Y., Wei, Y., et al. (2020). Single-cell transcriptomics identifies a distinct luminal progenitor cell type in distal prostate invagination tips. *Nature Genetics, 52*, 908–918.

Guo, W., Zhang, X., Li, L., Shao, P., Zhang, H., Liu, K., Liang, C., Wang, S., Peng, Y., Ju, Y., et al. (2023). *Intermediate basal cell population in prostate homeostasis and cancer initiation*, Article 540502, 2023.2005.2012.

Han, M., Li, F., Zhang, Y., Dai, P., He, J., Li, Y., Zhu, Y., Zheng, J., Huang, H., Bai, F., et al. (2022). FOXA2 drives lineage plasticity and KIT pathway activation in neuroendocrine prostate cancer. *Cancer Cell, 40*, 1306–1323.e1308.

Han, X., Wang, Y., Pu, W., Huang, X., Qiu, L., Li, Y., Yu, W., Zhao, H., Liu, X., He, L., et al. (2019). Lineage tracing reveals the bipotency of SOX9(+) hepatocytes during liver regeneration. *Stem Cell Reports, 12*, 624–638.

Han, X., Zhang, Z., He, L., Zhu, H., Li, Y., Pu, W., Han, M., Zhao, H., Liu, K., Li, Y., et al. (2021). A suite of new Dre recombinase drivers markedly expands the ability to perform intersectional genetic targeting. *Cell Stem Cell, 28*, 1160–1176 e1167.

He, L., Li, Y., Li, Y., Pu, W., Huang, X., Tian, X., Wang, Y., Zhang, H., Liu, Q., Zhang, L., et al. (2017). Enhancing the precision of genetic lineage tracing using dual recombinases. *Nature Medicine, 23*, 1488–1498.

He, L., Pu, W., Liu, X., Zhang, Z., Han, M., Li, Y., Huang, X., Han, X., Li, Y., Liu, K., et al. (2021). Proliferation tracing reveals regional hepatocyte generation in liver homeostasis and repair. *Science, 371*.

Karthaus, W. R., Iaquinta, P. J., Drost, J., Gracanin, A., van Boxtel, R., Wongvipat, J., Dowling, C. M., Gao, D., Begthel, H., Sachs, N., et al. (2014). Identification of multipotent luminal progenitor cells in human prostate organoid cultures. *Cell, 159*, 163–175.

Kruithof-de Julio, M., Shibata, M., Desai, N., Reynon, M., Halili, M. V., Hu, Y. P., Price, S. M., Abate-Shen, C., & Shen, M. M. (2013). Canonical Wnt signaling regulates Nkx3.1 expression and luminal epithelial differentiation during prostate organogenesis. *Developmental Dynamics, 242*, 1160–1171.

Kwon, O. J., Zhang, L., Ittmann, M. M., & Xin, L. (2014). Prostatic inflammation enhances basal-to-luminal differentiation and accelerates initiation of prostate cancer with a basal cell origin. *Proceedings of the National Academy of Sciences of the U S A, 111*, E592–E600.

Labrecque, M. P., Coleman, I. M., Brown, L. G., True, L. D., Kollath, L., Lakely, B., Nguyen, H. M., Yang, Y. C., da Costa, R. M. G., Kaipainen, A., et al. (2019). Molecular profiling stratifies diverse phenotypes of treatment-refractory metastatic castration-resistant prostate cancer. *Journal of Clinical Investigation, 129*, 4492–4505.

Li, J. J., & Shen, M. M. (2019). Prostate stem cells and cancer stem cells. *Cold Spring Harb Perspect Med, 9*.

Liu, X., Grogan, T. R., Hieronymus, H., Hashimoto, T., Mottahedeh, J., Cheng, D., Zhang, L., Huang, K., Stoyanova, T., Park, J. W., et al. (2016). Low CD38 identifies progenitor-like inflammation-associated luminal cells that can initiate human prostate cancer and predict poor outcome. *Cell Reports, 17*, 2596–2606.

Liu, K., Tang, M., Jin, H., Liu, Q., He, L., Zhu, H., Liu, X., Han, X., Li, Y., Zhang, L., et al. (2020). Triple-cell lineage tracing by a dual reporter on a single allele. *Journal of Biological Chemistry, 295*, 690–700.

Ma, Z., Lytle, N. K., Chen, B., Jyotsana, N., Novak, S. W., Cho, C. J., Caplan, L., Ben-Levy, O., Neininger, A. C., Burnette, D. T., et al. (2022). Single-cell transcriptomics reveals a conserved metaplasia Program in pancreatic injury. *Gastroenterology, 162*, 604–620.e620.

Madisen, L., Zwingman, T. A., Sunkin, S. M., Oh, S. W., Zariwala, H. A., Gu, H., Ng, L. L., Palmiter, R. D., Hawrylycz, M. J., Jones, A. R., et al. (2010). A robust and high-throughput Cre reporting and characterization system for the whole mouse brain. *Nature Neuroscience, 13*, 133–140.

Mu, P., Zhang, Z., Benelli, M., Karthaus, W. R., Hoover, E., Chen, C. C., Wongvipat, J., Ku, S. Y., Gao, D., Cao, Z., et al. (2017). SOX2 promotes lineage plasticity and antiandrogen resistance in TP53- and RB1-deficient prostate cancer. *Science, 355*, 84–88.

Ousset, M., Van Keymeulen, A., Bouvencourt, G., Sharma, N., Achouri, Y., Simons, B. D., & Blanpain, C. (2012). Multipotent and unipotent progenitors contribute to prostate postnatal development. *Nature Cell Biology, 14*, 1131–1138.

Pignon, J. C., Grisanzio, C., Geng, Y., Song, J., Shivdasani, R. A., & Signoretti, S. (2013). p63-expressing cells are the stem cells of developing prostate, bladder, and colorectal epithelia. *Proceedings of the National Academy of Sciences of the U S A, 110*, 8105–8110.

Pletcher, A., & Shibata, M. (2022). Prostate organogenesis. *Development, 149*.

Pu, W., Zhu, H., Zhang, M., Pikiolek, M., Ercan, C., Li, J., Huang, X., Han, X., Zhang, Z., Lv, Z., et al. (2023). Bipotent transitional liver progenitor cells contribute to liver regeneration. *Nature Genetics, 55*, 651–664.

Sfanos, K. S., Yegnasubramanian, S., Nelson, W. G., & De Marzo, A. M. (2018). The inflammatory microenvironment and microbiome in prostate cancer development. *Nature Reviews Urology, 15*, 11–24.

Shen, M. M., & Abate-Shen, C. (2010). Molecular genetics of prostate cancer: New prospects for old challenges. *Genes Dev, 24*, 1967–2000.

Shibata, M., Epsi, N. J., Xuan, S., Mitrofanova, A., & Shen, M. M. (2020). Bipotent progenitors do not require androgen receptor for luminal specification during prostate organogenesis. *Stem Cell Reports, 15*, 1026–1036.

Song, H., Weinstein, H. N. W., Allegakoen, P., Wadsworth, M. H., Xie, J., Yang, H., Castro, E. A., Lu, K. L., Stohr, B. A., Feng, F. Y., et al. (2022). Single-cell analysis of human primary prostate cancer reveals the heterogeneity of tumor-associated epithelial cell states. *Nature Communications, 13*, 141.

Srinivas, S., Watanabe, T., Lin, C. S., William, C. M., Tanabe, Y., Jessell, T. M., & Costantini, F. (2001). Cre reporter strains produced by targeted insertion of EYFP and ECFP into the ROSA26 locus. *BMC Developmental Biology, 1*, 4.

Tika, E., Ousset, M., Dannau, A., & Blanpain, C. (2019). Spatiotemporal regulation of multipotency during prostate development. *Development, 146*.

Toivanen, R., & Shen, M. M. (2017). Prostate organogenesis: Tissue induction, hormonal regulation and cell type specification. *Development, 144*, 1382–1398.

van Leenders, G., Dijkman, H., Hulsbergen-van de Kaa, C., Ruiter, D., & Schalken, J. (2000). Demonstration of intermediate cells during human prostate epithelial differentiation in situ and in vitro using triple-staining confocal scanning microscopy. *Laboratory Investigation, 80*, 1251–1258.

van Leenders, G. J., Gage, W. R., Hicks, J. L., van Balken, B., Aalders, T. W., Schalken, J. A., & De Marzo, A. M. (2003). Intermediate cells in human prostate epithelium are enriched in proliferative inflammatory atrophy. *American Journal Of Pathology, 162*, 1529–1537.

Vickman, R. E., Franco, O. E., Moline, D. C., Vander Griend, D. J., Thumbikat, P., & Hayward, S. W. (2020). The role of the androgen receptor in prostate development and benign prostatic hyperplasia: A review. *Asian journal of urology, 7*, 191–202.

Wagner, D. E., & Klein, A. M. (2020). Lineage tracing meets single-cell omics: Opportunities and challenges. *Nature Reviews Genetics, 21*, 410–427.

Wang, Z. A., Mitrofanova, A., Bergren, S. K., Abate-Shen, C., Cardiff, R. D., Califano, A., & Shen, M. M. (2013). Lineage analysis of basal epithelial cells reveals their unexpected plasticity and supports a cell-of-origin model for prostate cancer heterogeneity. *Nature Cell Biology, 15*, 274–283.

Wang, X., Xu, H., Cheng, C., Ji, Z., Zhao, H., Sheng, Y., Li, X., Wang, J., Shu, Y., He, Y., et al. (2020). Identification of a Zeb1 expressing basal stem cell subpopulation in the prostate. *Nature Communications, 11*, 706.

Wuidart, A., Ousset, M., Rulands, S., Simons, B. D., Van Keymeulen, A., & Blanpain, C. (2016). Quantitative lineage tracing strategies to resolve multipotency in tissue-specific stem cells. *Genes Dev, 30*, 1261–1277.

Wuidart, A., Sifrim, A., Fioramonti, M., Matsumura, S., Brisebarre, A., Brown, D., Centonze, A., Dannau, A., Dubois, C., Van Keymeulen, A., et al. (2018). Early lineage segregation of multipotent embryonic mammary gland progenitors. *Nature Cell Biology, 20*, 666–676.

Zhang, L., Zhang, B., Han, S. J., Shore, A. N., Rosen, J. M., Demayo, F. J., & Xin, L. (2012). Targeting CreER(T2) expression to keratin 8-expressing murine simple epithelia using bacterial artificial chromosome transgenesis. *Transgenic Research, 21*, 1117–1123.

Zou, M., Toivanen, R., Mitrofanova, A., Floch, N., Hayati, S., Sun, Y., Le Magnen, C., Chester, D., Mostaghel, E. A., Califano, A., et al. (2017). Transdifferentiation as a mechanism of treatment resistance in a mouse model of castration-resistant prostate cancer. *Cancer Discovery, 7*, 736–749.